JOURNAL OF CATALYSIS **160,** 106–117 (1996)
ARTICLE NO. 0128

Effect of In and Sn on the Adsorption Behavior and Hydrogenolysis Activity of Pt/Al_2O_3 Catalysts

Fabio B. Passos,[1] Martin Schmal,* and M. A. Vannice†,[2]

*NUCAT/COPPE–Universidade Federal do Rio de Janeiro, Caixa Postal 68502, Rio de Janeiro, RJ, 21945-970, Brazil; and
† Department of Chemical Engineering, Pennsylvania State University, University Park, Pennsylvania 16802

Received August 23, 1995; revised January 25, 1996; accepted January 26, 1996

The influence of Sn and In on the properties of Pt/Al_2O_3 catalysts was investigated. Integral heats of adsorption, Q_{ad}, for H_2 at 300 K were determined on a group of Pt, Pt–Sn, and Pt–In/Al_2O_3 catalysts. Although H_2 chemisorption was significantly suppressed in the case of the bimetallic catalysts, the irreversible Q_{ad} values were typically decreased to a lesser extent and fell between 10.6 and 13.3 kcal/mol, which is slightly lower than the range of values previously measured for H_2 adsorption on Pt. The presence of these two promoters also decreased the amount of CO adsorbed at 300 K; however, the irreversible heats of CO adsorption were essentially not altered by the presence of either Sn or In as the Q_{ad} values were 23 ± 2 kcal/mol and consistent with values previously measured for Al_2O_3-supported Pt. DRIFTS measurements at 300 K implied that surface Pt atoms were more homogeneously diluted or covered by In than by Sn. Thermal desorption experiments in the DRIFTS cell showed that the IR vibration for CO species adsorbed on on-top sites was 2042 ± 3 cm^{-1} at low coverage for all the samples investigated. The turnover frequency (TOF) for *n*-butane hydrogenolysis on Pt/Al_2O_3 was decreased by the addition of either Sn or In, but the largest variation occurred with Pt–In/Al_2O_3, which gave TOF values at 573 K up to 40 times lower than those for Pt/Al_2O_3 catalysts. The results can be explained by a *geometric* effect in which the number of contiguous Pt atoms is decreased by dilution with either Sn or In atoms, i.e., ensemble size decreases, and any electronic effects appear to play only a minor role. The variations in butane hydrogenolysis are consistent with DRIFTS results, in that the dilution of Pt surface atoms by In atoms seems to be more homogeneous thus causing a more effective suppression of hydrogenolysis activity.

INTRODUCTION

A change in the adsorption properties of an active metal has frequently been used as an explanation for a promoter effect of an inert metal in bimetallic catalysts. In particular, supported Pt-based catalysts have been thoroughly investigated due to their tremendous importance in the petroleum and petrochemical industries (1–3). Two main explanations—geometric and electronic—have been proposed in the literature to explain the catalytic behavior of these catalysts. The geometric effect states that there is a decrease in the number of Pt atoms in the ensemble constituting an active site for the formation of coke precursors or for the progress of undesirable structure-sentitive reactions (4). On the other hand, the electronic effect proposes that there is a decrease in the strength of the bond between the adsorbed hydrocarbons and the surface metal atoms, caused by a change in the electronic properties of platinum (5).

Despite these considerations, heats of adsorption of gases on these Al_2O_3-supported catalysts are not available in the literature; therefore, in this study we conducted calorimetric measurements of H_2 and CO adsorption on alumina-supported Pt–Sn and Pt–In catalysts using a modified differential scanning calorimeter. This technique has been successfully employed for the determination of integral, isothermal heats of adsorption on supported Pt catalysts (6–8). It avoids the problems of readsorption and diffusion present when TPD methods are used with porous catalysts, and the collection of data is fast and reproducible. In addition, diffuse reflectance infrared fourier transform spectroscopy (DRIFTS) was employed to study the state of CO on the surface of these catalysts. Shifts and changes in the spectra obtained by infrared spectroscopy of adsorbed CO have been previously used in an argument to explain the electronic nature of any promotion mechanism (9).

Finally, we have conducted a probe reaction, the hydrogenolysis of *n*-butane, which is sensitive to the surface structure of the metal particles in these catalysts (10–13). Hydrogenolysis reactions are also parasitic reactions in industrial reforming processes, and a good promoter should be able to inhibit the occurrence of such reactions. Therefore, a comparison among the performances of the catalysts could provide additional information on the mechanism of promotion.

One more statement is required about the choice of In and Sn as promoters. They are both additives in a Pt-based,

[1] Permanent address: Departamento de Engenharia Quimica, Universidade Federal Fluminense, R. Passo da Pátria, 156, Niterói, RJ, 24210-230, Brazil.

[2] To whom correspondence should be addressed.

0021-9517/96 $18.00

Al_2O_3-supported multimetallic catalyst used in a process for dehydrogenation of long-chain alkanes (C_9–C_{14}) to form α-olefins (14). Several studies (15–19) have focused on the effect of Sn in Pt–Sn catalysts, but there is still interest in determining the differences between Sn and In. Only two studies of Pt–In systems have been reported (20, 21) and further investigation is necessary.

EXPERIMENTAL

Al_2O_3 (Harshaw Al3996R, 200 m^2/g) was used as the support material in this study. Pt/Al_2O_3 catalysts were prepared by an incipient wetness technique using an aqueous solution of H_2PtCl_6 (0.7 cm^3/g) followed by drying at 393 K for 16 h and calcination in air at 773 K for 2 h. The bimetallic $Pt–In/Al_2O_3$ and $Pt–Sn/Al_2O_3$ catalysts were prepared in three distinct ways, using $In(NO_3)_3$ and $SnCl_2$ as precursors:

(a) The $(Pt + X)/Al_2O_3$ (X = Sn or In) catalysts were prepared by coimpregnation of the Al_2O_3 at 300 K with an aqueous solution containing both metallic precursors. After the impregnation, the sample was dried in air at 393 K for 16 h.

(b) The $X + (Pt/Al_2O_3)$ catalysts were prepared by reimpregnation of the Pt/Al_2O_3 catalyst after the calcination step with an aqueous solution of the second metal precursor, followed by drying in air at 393 K for 16 h.

(c) The $Pt + (X/Al_2O_3)$ catalysts were prepared by reimpregnation of the X/Al_2O_3 samples with an H_2PtCl_6 aqueous solution after the calcination step, followed by the drying step.

The dried samples were ground and calcined in air at 773 K for 2 h. The prepared catalysts and the chemical compositions measured by atomic absorption are listed in Table 1.

The gases used in this study—H_2 (MG Ind., 99.999%), He (MG Ind., 99.999%), and Ar (MG Ind., 99.999%)—were further purified by passage through 5A molecular sieve (Supelco) and through Oxytraps (Alltech Assoc.). CO (Matheson, 99.99%) was passed through a 5A molecular sieve (Supelco). Hydrogen and carbon monoxide uptakes were measured in a stainless-steel adsorption system equipped with a Balzers TSU-171 turbomolecular pump that provided a vacuum below 10^{-6} Torr at the sample. Isotherm pressures were obtained using a MKS Baratron Model 310 capacitance manometer. The pretreatment of the catalysts consisted of drying at 393 K under a He flow, reduction in a 10% H_2/90% He mixture at 533 K for 30 min, and a final reduction at 723 K for 1 h. Then, all samples were evacuated for 1 h at 698 K before cooling in vacuum to 300 K, where all chemisorption measurements were made. After the initial adsorption isotherm, the samples were evacuated for 30 min at 300 K and a second isotherm was obtained to determine reversible adsorption.

The calorimetric measurements were performed in a modified Perkin–Elmer DSC-2C differential scanning calorimeter operated isothermally. All gas flows were controlled by mass flow controllers (Tylan Model FC260), and a complete description of the apparatus has been provided elsewhere (7). Before isothermal measurements in the DSC, the same pretreatment used in the chemisorption experiments was employed, except that the reduction was done under a 10% H_2/90% Ar flow and a 1-h purge with He

TABLE 1

Chemical Composition and Hydrogen Uptakes on Pt Catalysts at 300 K

Catalyst	Pt content (wt%)	Sn content (wt%)	In content (wt%)	H_2 uptake[a] (μmol/gcat) Total	Irrev.	H/Pt[b]
Pt/Al_2O_3	0.69	—	—	24.8	16.5	0.93
18.5% Pt/Al_2O_3	18.5	—	—	312	233	0.49
18.5% Pt/Al_2O_3(S)[c]	18.5	—	—	24.0	15.0	0.03
$(Pt + In)/Al_2O_3$	0.66	—	0.81	12.3	7.4	0.44
$In + (Pt/Al_2O_3)$	0.71	—	0.78	16.8	10.7	0.59
$Pt + (In/Al_2O_3)$	0.68	—	0.80	17.6	11.0	0.63
$(Pt + In)/Al_2O_3$(B)[d]	0.66	—	0.81	11.7	5.4	0.32
$In + (Pt/Al_2O_3)$(B)[d]	0.71	—	0.78	11.9	5.8	0.32
$Pt + (In/Al_2O_3)$(B)[d]	0.68	—	0.80	16.3	9.2	0.53
$(Pt + Sn)/Al_2O_3$	0.92	0.73	—	18.8	11.3	0.48
$Sn + (Pt/Al_2O_3)$	0.95	0.87	—	17.7	10.3	0.45
$Pt + (Sn/Al_2O_3)$	0.89	0.82	—	20.2	12.1	0.53
Pt powder	100	—	—	3.0	1.9	7.4×10^{-4}

[a] Uptakes obtained at 123 Torr.
[b] Values based on irreversible H_2 uptake.
[c] Sintered at 973 K for 2 h in 20% O_2.
[d] Subjected to a second reduction cycle.

was employed in lieu of the 1-h evacuation step. Hydrogen exotherms were obtained at 123 Torr, with the base He carrier gas flowing at 35.0 $cm^3\ min^{-1}$, while the makeup stream was switched from 10.5 $cm^3\ min^{-1}$ He to 7.0 $cm^3\ min^{-1}$ H_2. A purge time of 1 h at 35.0 $cm^3\ min^{-1}$ He was used between the first and the second exotherm experiments. CO exotherms were obtained at 73 Torr and the makeup stream was switched from 0.4 $cm^3\ min^{-1}$ He to 3.9 $cm^3\ min^{-1}$ CO. A purge time of 1 h at 35.0 $cm^3\ min^{-1}$ Ar was used between the first and the second exotherm experiments. The energy changes were measured using a similar mass of nonporous glass beads in the reference side of the calorimeter.

Infrared measurements were conducted in a Sirius 100 FTIR (Mattson Inst.) using a diffuse reflectance cell (HVC-DRP, Harrick Sci.) that has been modified to allow *in situ* treatments (22). The flow rates of the gases were measured and controlled by Tylan FC260 mass flow controllers. The powder samples were loaded without a diluent into the diffuse reflectance cell which was then attached to the spectrometer. The pretreatment of the samples was identical to that used in the calorimetric experiments. After the purge step, a standard procedure was employed to collect the interferograms at several temperatures. Under 36.0 $cm^3\ min^{-1}$ Ar flow, interferograms were obtained at the following temperatures: 723, 673, 623, 573, 523, 473, 423, 373, and 298 K. These interferograms were later used as the background references to obtain spectra at each temperature. After taking the background interferogram at 298 K, a 10% CO/90% Ar mixture was admitted into the cell for 15 min at 40 $cm^3\ min^{-1}$. The sample was purged with Ar for 30 min, and interferograms were taken first at 298 K, then at each temperature at which a reference interferogram had been taken. The interferograms were obtained after 1000 scans taken with a preamplifier gain of 4, an iris setting of 50%, and 4 cm^{-1} resolution. The data points were stored in a 486 DX-33 personal computer, and then using data processing software (Mattson WinFIRST), each sample or reference interferogram was Fourier transformed to its equivalent frequency component spectrum and the ratio of these two spectra gave the transmittance spectrum, from which the absorbance spectrum was obtained. The spectra were represented in both absorbance and Kubelka–Munk (K-M) units and both sets were routinely very similar. The former representation is preferred because negative intensity changes appear as positive peaks in K-M units.

The vapor-phase hydrogenolysis experiments were performed in an atmospheric glass microreactor. The gas flows were controlled and measured by calibrated mass flow controllers (Tylan FC260). The amount of catalyst loaded into the reactor was varied from 50 to 250 mg in such way to keep conversions lower than 10% (in most cases below 5%). The reactant mixture consisted of hydrogen (36 $cm^3\ min^{-1}$) and *n*-butane (4 $cm^3\ min^{-1}$) with a molar ratio of 9 : 1. The pretreatment of the catalysts consisted of drying at 393 K for 30 min under flowing He, followed by reduction in 10% H_2/90% He at 723 K for 1 h. Then each catalyst was cooled to the reaction temperature where the H_2 flow rate was adjusted before the introduction of *n*-C_4H_{10}. Arrhenius plots were obtained between 520 and 615 K. In these runs, an ascending temperature sequence was followed by a descending temperature sequence in order to detect any deactivation. A bracketing technique (1, 23) with pure H_2 was used while changing the temperatures. The reactor effluent was analyzed by on-line gas chromatography using a H-P 5730A chromatograph equipped with a flame ionization detector and a 6-ft column containing 80/100 mesh Chemipack C-18 (Alltech).

Besides the reaction rate for total hydrogenolysis (r), rates of terminal (r_t) and central (r_c) bond scission were determined by considering, respectively, the conversion of butane to methane plus propane and the conversion of butane to ethane (12). The selectivities to methane, ethane and isobutane were calculated accordingly to

$$\text{Selectivity to } i = \frac{\text{molar amount of butane converted to } i}{\text{total molar amount of butane converted}}.$$

RESULTS

Total and irreversible hydrogen uptakes at 300 K and the corresponding H/Pt ratios for irreversible adsorption are listed in Table 1. Representative isotherms for H_2 on Pt/Al_2O_3, $(Pt + In)/Al_2O_3$, and $(Pt + Sn)/Al_2O_3$ are plotted in Fig. 1. The listed uptakes were obtained from the isotherms and correspond to the same partial pressure used in the calorimetric experiments. The presence of indium and tin caused similar decreases in the H/Pt ratio, with values ranging from 0.32 to 0.63. No attempt was made to calculate the Pt particle size from the H/Pt ratios because it is known that the observed decrease in H/Pt ratios for these bimetallic catalysts is not due to an increase in particle size (17). The catalysts in the B series were submitted to two successive cycles of reduction and adsorption, separated by exposure to air at room temperature, and it can be seen that some decline in the uptakes occurred compared to those after the initial cycle. Thus, *exactly* identical adsorption and energy change sequences are required to obtain accurate results for the bimetallic catalysts. $(Pt + In)/Al_2O_3$ presented the lowest H/Pt ratio among the Pt–In catalysts, while the catalysts prepared by successive impregnation presented similar H_2 uptakes. The method of impregnation did not seem to have any significant effect on H_2 uptake of the Pt–Sn catalysts.

Table 2 shows the total and reversible energy changes measured during hydrogen adsorption and the calculated total and irreversible heats of hydrogen adsorption. The total Q_{ad} values include reversible H_2 adsorption on both the Pt and the Al_2O_3 surfaces as well as irreversible H_2

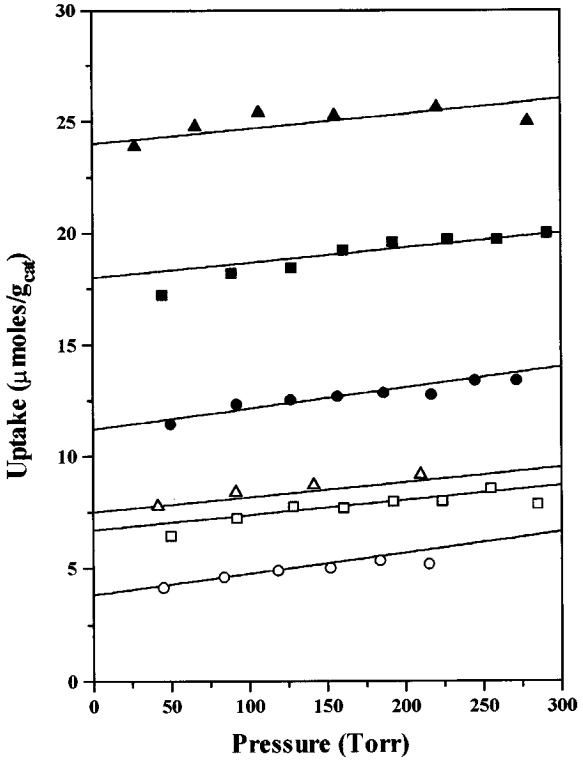

FIG. 1. Adsorption isotherms for hydrogen on Pt/Al_2O_3 (triangles), $(Pt + In)/Al_2O_3$ (circles), and $(Pt + Sn)Al_2O_3$ (squares). $T = 300$ K: total H_2, closed symbols; reversible H_2, open symbols.

adsorption on the Pt. Typical exotherms obtained for H_2 adsorption on Pt/Al_2O_3 are shown in Fig. 2. The Q_{ad} values for irreversible H_2 adsorption on the 0.7% Pt/Al_2O_3 catalyst was 13.3 kcal/mol (1 kcal = 4.18 kJ) as in an earlier study (8). The Q_{ad} values were not a function of platinum particle size: 0.7% Pt/Al_2O_3, 18.5% Pt/Al_2O_3, 18.5% Pt/Al_2O_3(S), and Pt powder gave very similar values, with an average of 14.0 ± 0.7 kcal/mol. The respective Q_{ad} values for irreversible hydrogen adsorption on the bimetallic catalysts were in the same range, but most of them were somewhat lower; for example, the average value (with standard deviation) for the Pt–In catalysts was 11.8 ± 1.3 kcal/mol, while an average value of 11.7 ± 1.4 kcal/mol was obtained with the Pt–Sn catalysts.

CO uptakes and heats of adsorption on the catalysts are listed in Table 3, while representative isotherms of CO adsorption on Pt/Al_2O_3, $(Pt + In)/Al_2O_3$, and $(Pt + Sn)/Al_2O_3$ are shown in Fig. 3, and typical exotherms obtained with Pt/Al_2O_3 are shown in Fig. 4. CO uptakes were lower on the bimetallic catalysts, in agreement with the results for H_2 adsorption as shown by the CO/H ratio being always near 1. The integral heat of adsorption for CO on Pt/Al_2O_3 at 300 K was 23.9 kcal/mol and the other catalysts gave similar values, with an average and standard deviation of 23.5 ± 1.1 kcal/mol.

TABLE 2

Heats of Hydrogen Adsorption on Supported Platinum

Catalyst	Average energy change (mcal/g)		Q_{ad} (kcal/mol H_2)	
	Total	Rev.	Total	Irrev.
Pt/Al_2O_3	313.2	93.5	12.6	13.3
18.5% Pt/Al_2O_3	4493.0	1082.2	14.4	14.6
18.5% Pt/Al_2O_3(S)[a]	329.6	120.6	13.0	13.9
$(Pt + In)/Al_2O_3$	126.4	45.7	10.3	10.9
$In + (Pt/Al_2O_3)$	187.5	63.5	11.2	11.6
$Pt + (In/Al_2O_3)$	195.5	70.0	11.1	11.4
$(Pt + In)/Al_2O_3$(B)[b]	111.5	41.4	9.5	13.0
$In + (Pt/Al_2O_3)$(B)[b]	130.8	51.9	11.0	13.6
$Pt + (In/Al_2O_3)$(B)[b]	151.5	57.9	9.3	10.2
$(Pt + Sn)/Al_2O_3$	230.9	91.4	12.3	13.3
$Sn + (Pt/Al_2O_3)$	180.6	64.3	10.2	11.3
$Pt + (Sn/Al_2O_3)$	223.5	87.5	11.1	11.3
Pt powder	42.9	15.5	14.3	14.4

[a] Sintered at 973 K.
[b] Subjected to a second reduction cycle.

DRIFTS absorbance spectra of CO adsorbed at room temperature on several catalysts are shown in Fig. 5. The Pt/Al_2O_3 catalyst showed a main band with a maximum at 2063 cm^{-1}, a shoulder at 2075 cm^{-1}, and a tail in the 2000–2100 cm^{-1} range. A smaller band was also observed at 1835 cm^{-1} for this catalyst.

For the Pt–In catalysts, the main band shifted to lower wavenumbers, varying from 2053 to 2060 cm^{-1}. The Pt–Sn catalysts did not show any trend in comparison to Pt/Al_2O_3, as the main band maximum ranged from 2066 to 2056 cm^{-1}. The shoulder around 2075 cm^{-1} was not observed for the bimetallic samples and the low frequency band at 1835 cm^{-1} was suppressed for the Pt–In catalysts, but a small band was still observable in the case of Pt–Sn catalysts. Figures 6–8 show typical sets of infrared spectra taken at various temperatures for Pt/Al_2O_3, $(Pt + In)/Al_2O_3$, and $(Pt + Sn)/Al_2O_3$, respectively. For the Pt/Al_2O_3 catalysts there was an increase in the integrated intensity of the main peak when the temperature was increased from 300 to 473 K.

Figure 9 shows the change in the peak position of the main band with the CO surface coverage. The surface coverages were obtained by dividing the total integrated area of the CO vibration band at each temperature by the total integrated area obtained at room temperature and assuming that the extinction coefficient remained constant. The peak positions were normalized to the positions that would be observed if the spectra were taken at room temperature by calibration experiments that were performed to evaluate the influence of temperature on the peak position. These experiments consisted of taking a scan at a higher temperature and then taking scans at the same coverage at lower temperatures; thus these plotted points denoted only the

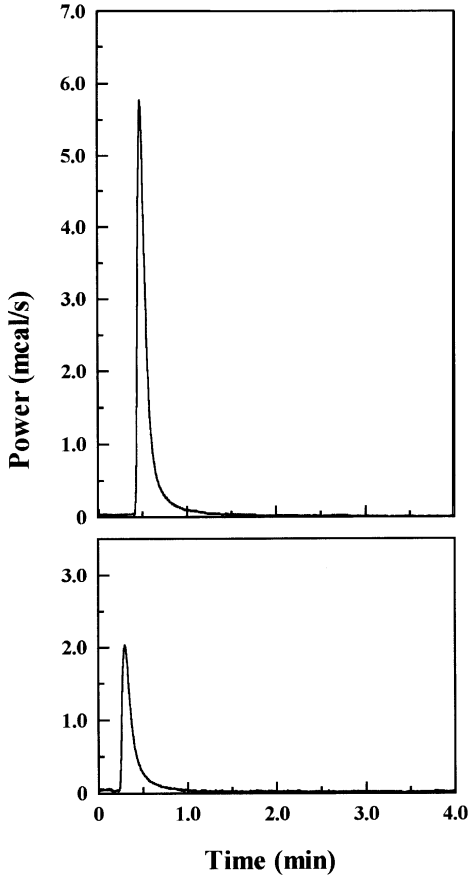

FIG. 2. Calorimeter exotherms for H_2 adsorption on Pt/Al_2O_3. $T = 300$ K, $P_{H_2} = 123$ Torr. Top, initial H_2 adsorption; bottom, reversible H_2 adsorption.

effect of temperature on the peak position. By extrapolating the curves to zero coverage, the singleton vibration for linearly adsorbed CO can be estimated (24). For all catalysts studied the singleton vibration frequencies were within 2042 ± 3 cm^{-1}.

Arrhenius plots for butane hydrogenolysis over Pt/Al_2O_3, $(Pt + In)/Al_2O_3$, and $(Pt + Sn)/Al_2O_3$, are presented in Fig. 10. The specific activities at 573 K and the activation energies obtained for butane hydrogenolysis over these catalysts are listed in Table 4. The turnover frequencies were obtained by using the irreversible H_2 uptake at 300 K to estimate the number of available surface Pt atoms. Specific activity for the hydrogenolysis of *n*-butane was suppressed by the presence of Sn and In; for example, depending on the preparative method, In suppressed the turnover frequencies from 5- to 40-fold, while the suppression by Sn was milder, with suppression factors ranging from 2- to 4-fold.

All the catalysts showed some deactivation, losing from 20 to 50% of their initial activity after a sojourn at temperatures above 590 K, and the bimetallic catalysts showed as much or more deactivation as the Pt/Al_2O_3 catalyst. The apparent activation energy for Pt/Al_2O_3 was equal to 35 kcal/mol during ascending temperature sequence, and it increased only 5 kcal/mol during the descending temperature sequence. In most cases, the bimetallic catalysts presented similar activation energies, with an average value of 33 ± 6 kcal/mol during the ascending temperatures sequence, and an average value of 37 ± 4 kcal/mol during the descending

TABLE 3

CO Adsorption on Supported Pt at 300 K

Catalyst	CO uptake[a] (μmol/g) Total	Irrev.	CO/H[b]	Energy change (mcal/g) Total	Rev.	Q_{ad} (kcal/mol CO) Irrev.
Pt/Al_2O_3	52.0	34.0	1.0	928.2	114.2	23.9
$(Pt + In)/Al_2O_3$	35.6	16.0	1.1	481.4	99.7	23.9
$In + (Pt/Al_2O_3)$	37.7	23.0	1.1	643.2	98.9	23.7
$Pt + (In/Al_2O_3)$	41.0	23.0	1.0	636.1	122.1	22.3
$(Pt + Sn)/Al_2O_3$	40.5	27.0	1.2	725.3	133.9	21.9
$Sn + (Pt/Al_2O_3)$	41.0	24.0	1.2	708.1	115.1	24.7
$Pt + (Sn/Al_2O_3)$	49.1	28.0	1.2	824.6	143.9	24.3

[a] Uptakes obtained at 73 Torr.
[b] Values based on irreversible uptakes.

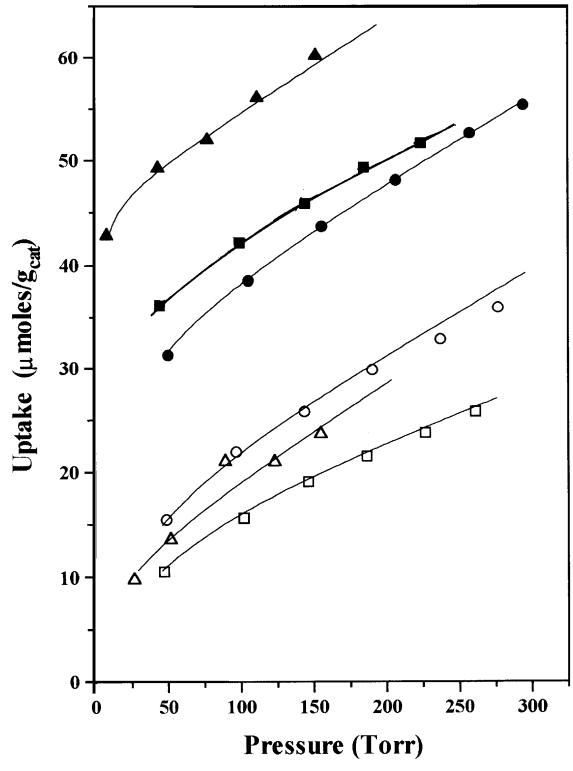

FIG. 3. Adsorption isotherms for carbon monoxide on Pt/Al_2O_3 (triangles), $(Pt + In)/Al_2O_3$ (circles), and $(Pt + Sn/Al_2O_3)$ (squares). $T = 300$ K: total H_2, closed symbols; reversible H_2, open symbols.

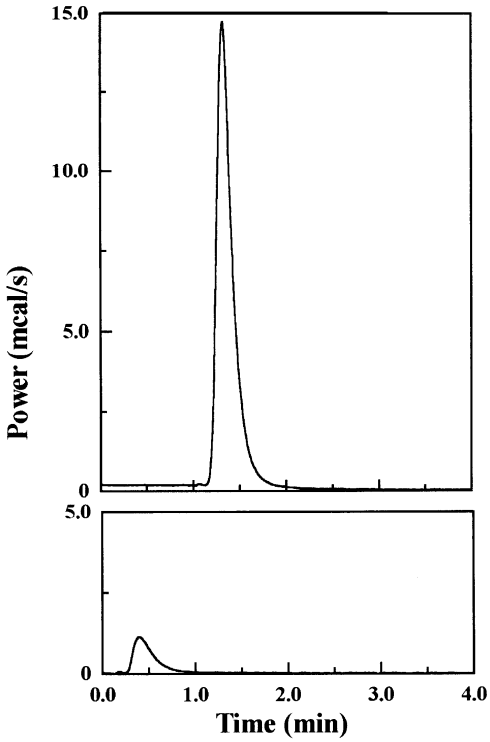

FIG. 4. Calorimeter exotherms for CO adsorption on Pt/Al_2O_3. $T = 300$ K, $P_{CO} = 123$ Torr. Top, initial H_2 adsorption; bottom, reversible H_2 adsorption.

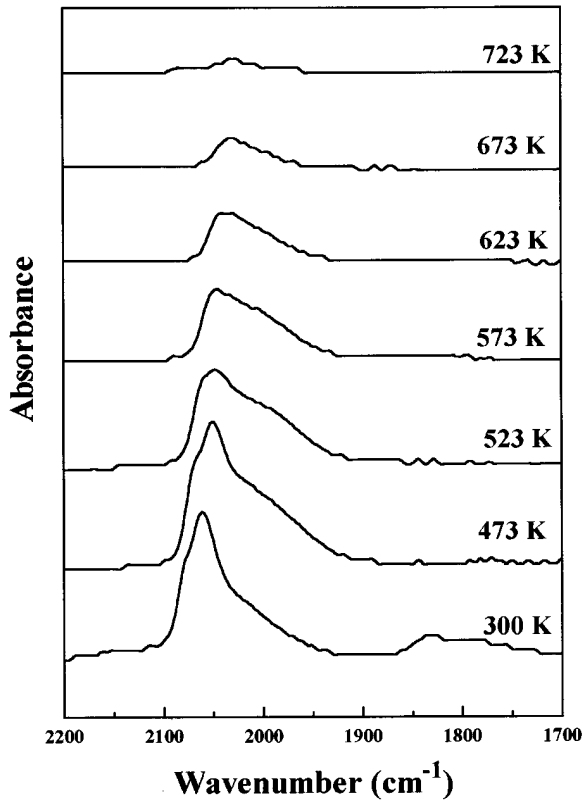

FIG. 6. Thermal desorption infrared spectra of CO adsorbed on Pt/Al_2O_3.

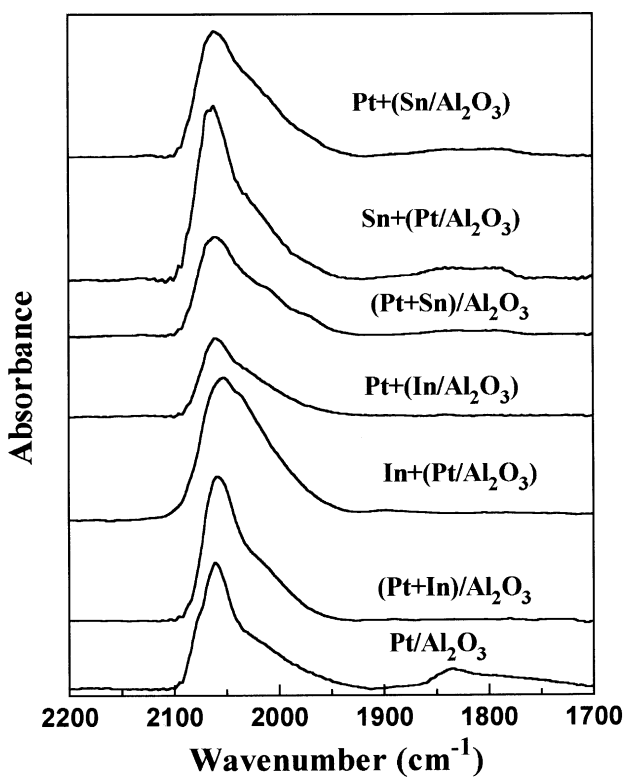

FIG. 5. Infrared spectra of adsorbed CO at room temperature on Pt, Pt–Sn, and Pt–In/Al_2O_3 catalysts.

temperature sequence. The product distribution at 573 K is given in Table 5. The selectivity for isomerization was lowest for the Pt/Al_2O_3 catalyst, remained low for Pt–Sn/Al_2O_3 catalysts, and was highest for the catalysts containing In, especially the In + (Pt/Al_2O_3) sample. The C_1/C_3 mole ratio in the products, which monitors the extent of multiple hydrogenolysis of butane, is also reported. For all the catalysts this ratio was approximately 1, indicating that only a single hydrogenolysis step occurred. A comparison between terminal and central bond breaking in the various catalysts is displayed in Table 6. The rates of these reactions at 573 K, their respective ratio, r_t/r_c, and the activation energies obtained from the ascending and descending temperature sequences are also listed. For the Pt/Al_2O_3 catalyst, the r_t/r_c ratio was equal to 2.2 before the increase in the temperature, and after the descending temperature sequence this ratio increased to 3.0, indicating some preferential deactivation of the rate for central bond scission of *n*-butane. Similar results were obtained with most of the bimetallic catalysts, for which r_t/r_c usually went up after a sequence of measurements at several temperatures. Compared to Pt alone, the effect of Sn on the r_t/r_c ratio was small, while the effect of In was a function of preparative method: the coimpregnated (Pt + In)/Al_2O_3 showed a lower value than Pt/Al_2O_3, no

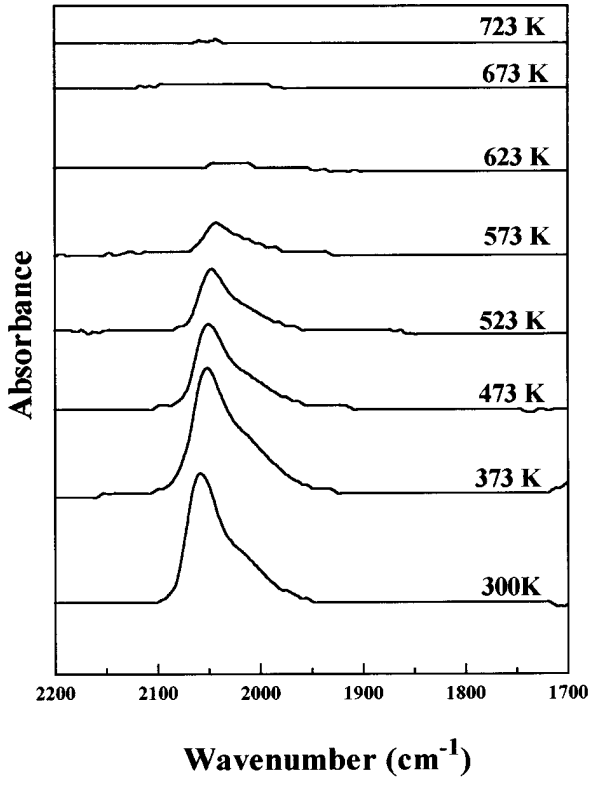

FIG. 7. Thermal desorption infrared spectra of CO adsorbed on $(Pt + In)/Al_2O_3$.

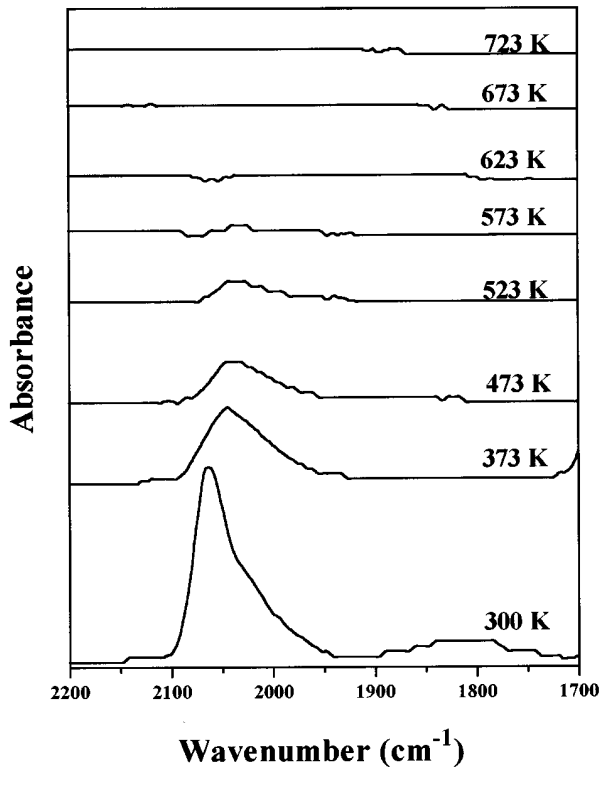

FIG. 8. Thermal desorption infrared spectra of CO adsorbed on $(Pt + Sn)/Al_2O_3$.

change was observed for $Pt + (In/Al_2O_3)$, and a increase in the r_t/r_c ratio was observed in the case of $In + (Pt/Al_2O_3)$.

DISCUSSION

It is well established that the surface compositions of these catalysts are complex and they can depend on the support and its surface area, the Pt/Sn ratio, and the method of preparation (5, 15, 25–28). The formation of Pt–Sn alloys (15), the stabilization of Sn^{+2} at the alumina surface (5, 25), and the presence of both forms of tin (26) have been reported. Similar results have been observed in the Pt–In system (27). We, as others before us, cannot give a complete description of the physical distribution of Sn or In or the distribution of oxidation states of either of these components in these catalysts; however, the integrated effect of each additive on Pt can be probed by the combination of H_2 and CO heats of adsorption, the IR peak shifts, and the n-C_4 hydrogenolysis behavior obtained in this study.

The heat of H_2 adsorption observed for the Pt/Al_2O_3 catalysts is consistent with the values previously reported for Pt dispersed in a variety of supports, which averaged 13.5 ± 2 kcal/mol for saturation coverage (total adsorption) and 16.2 ± 3 kcal/mol for irreversible adsorption (6). The irreversible Q_{ad} may be subject to higher experimental error as it is determined indirectly; however, this value is more appropriate for comparison because the total adsorption exotherm includes the reversible adsorption on the Al_2O_3 as well as on the Pt. The irreversible Q_{ad} is in agreement with values obtained for Pt dispersed on SiO_2 (8, 29, 30) and it is consistent with studies on single crystals (31–37) and metal films (38, 39) that have been previously compared (6).

The decrease in the H/Pt ratio for the $Pt–Sn/Al_2O_3$ and $Pt–In/Al_2O_3$ catalysts can be regarded as an indication of the interaction between Pt and Sn or In. It is not expected to be caused by a decrease in the dispersion of the Pt particles, i.e., crystallite growth, and, in fact, EXAFS studies have shown that Pt is more dispersed on alumina when Sn is present (25). The decline in H_2 chemisorption could be caused either by the introduction of inert In or Sn atoms between Pt atoms or by the physical blockage of platinum atoms due to overlayer formation, as either possibility could inhibit dissociative H_2 adsorption. Another explanation could invoke a *ligand* effect, which could cause a lowering of the heat of adsorption of hydrogen on platinum. Our results tend to favor the first hypothesis because the hydrogen heats of adsorption were either unchanged or the change not large and, although most of the bimetallic catalysts did show a small decrease in their Q_{ad} value, this could be due to preferential coverage of high binding sites on the Pt surface by the Sn or In atoms.

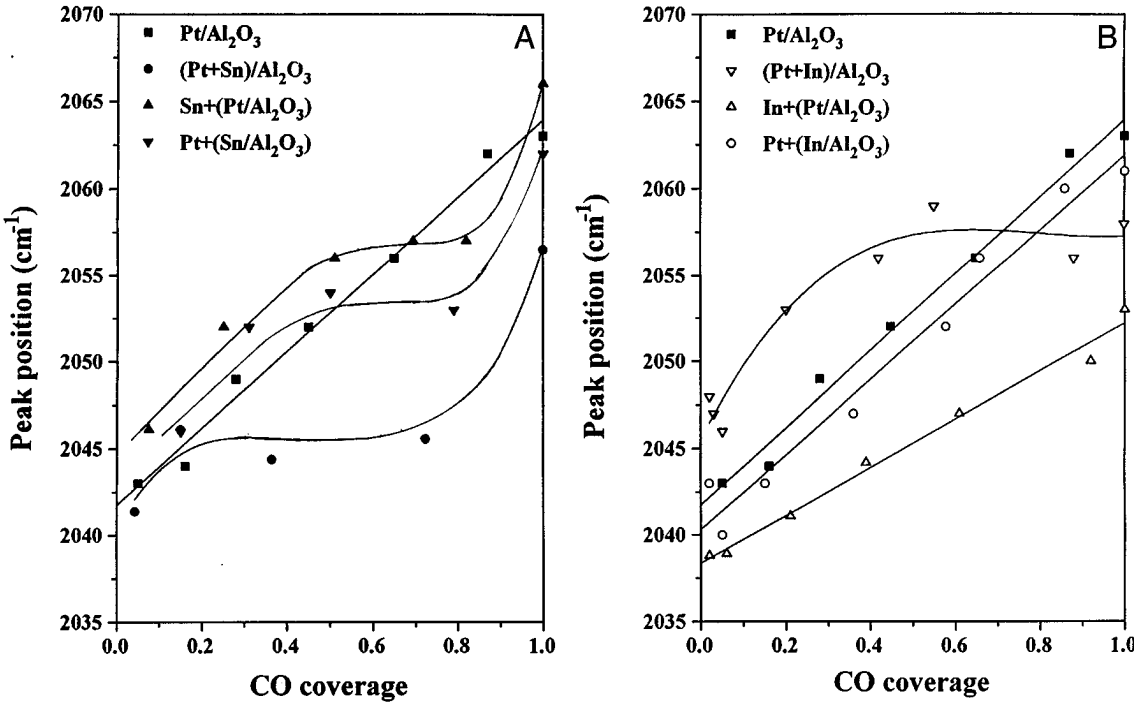

FIG. 9. Infrared peak positions at 300 K of linearly bonded CO for varying surface coverages after correction for thermal effects: (A) $Pt–Sn/Al_2O_3$ catalysts; (B) $Pt–In/Al_2O_3$ catalysts.

Reports of heats of adsorption of hydrogen on supported, bimetallic Pt catalysts and studies of unsupported alloy surfaces are scarce. Paffett *et al.* investigated H_2 adsorption at 150 K on ordered Sn/Pt(111) alloy surfaces and noticed a large inhibition of the hydrogen uptake compared to Pt(111), but they could not determine accurate activation energies for the dissociative adsorption of hydrogen (40). This suppression of dissociative H_2 adsorption was attributed primarily to a geometric effect, i.e., the removal of contiguous Pt three-fold hollow sites (40). They estimated that if the activation energy were near the minimum value required to cause the hydrogen inhibition, the Pt–H bond strength would not be changed by alloying with Sn. Cortright and Dumesic (28) investigated H_2 adsorption on $Pt–Sn/SiO_2$ catalysts by calorimetry and found the heat of H_2 adsorption was not changed, compared to a Pt/SiO_2 catalyst, when the Pt/Sn atomic ratio was 1 or 6, but there was a decrease in the Q_{ad} value for the catalyst with an atomic Pt/Sn ratio of 1/6. In short, the available results seem to indicate that the main effect of In or Sn addition on H_2 adsorption is geometric, though we cannot discard the possibility that minor electronic changes in the Pt may occur that have a small influence on the integral heats of adsorption. This premise that a geometric effect dominates is consistent with the results for CO adsorption and with the kinetic data for the hydrogenolysis of *n*-butane.

The adsorption of CO on platinum surfaces has been extensively investigated in the literature. Heats of CO adsorption on single crystals (31, 41–53), foils (54), and films (55) have been compared previously (8), and the values range from 25 to 35 kcal/mol. CO heats of adsorption on supported platinum collected from the literature are shown in Table 7. The heat of CO adsorption on our Pt/Al_2O_3 catalyst was 23.9 kcal/mol, which is in excellent agreement with the values reported earlier for well-dispersed $Pt/\eta–Al_2O_3$ (8, 56) and is higher than the 18 kcal/mol measured by TPD (57). As observed before, the values for Pt supported on Al_2O_3 are somewhat lower than those obtained with Pt/SiO_2, indicating some sort of support effect.

CO heats of adsorption on $Pt–Sn/SiO_2$ have been recently reported by Cortright and Dumesic (28). As observed with H_2 adsorption, a decrease in the CO heat of adsorption was observed only for the catalyst with an atomic Pt–Sn ratio equal to 1/3. Verbeek and Sachtler (61) examined PtSn and Pt_3Sn bulk alloys by TPD of adsorbed CO and found there was only a small difference between the temperature of maximum CO desorption on Pt_3Sn and pure Pt powder. However, a larger shift in the TPD peak position was observed for PtSn, indicating a *ligand* effect when there was an increase in the amount of Sn in the alloy. For linearly adsorbed CO on Pt(111), a heat of adsorption equal to 29 kcal/mol was observed by thermal desorption, and a decrease of 5 kcal/mol in the CO heat of adsorption was estimated for Sn/Pt(111) alloy surfaces (40). No change in the heat of adsorption was observed for CO adsorbed in the bridged form. Our results did not show any trend with the

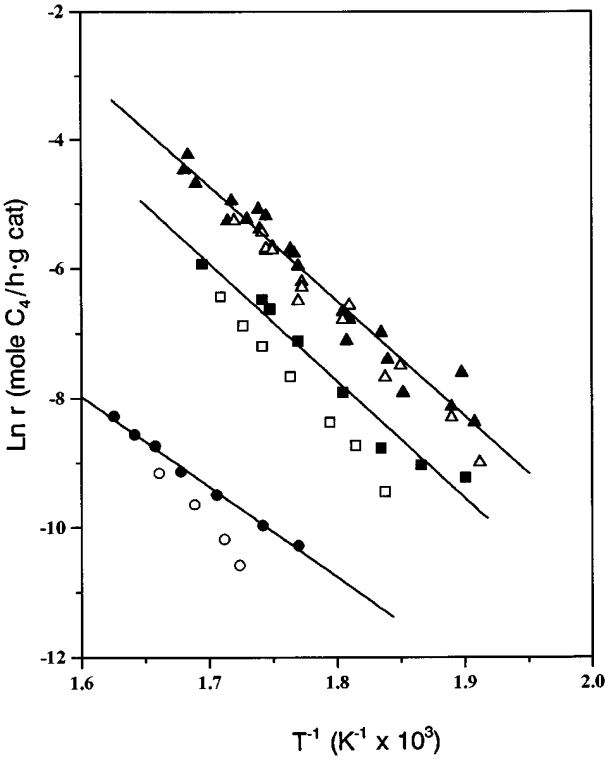

FIG. 10. Arrhenius plots for butane hydrogenolysis over Pt/Al_2O_3 (triangles), $(Pt + In)/Al_2O_3$ (circles), and $(Pt + Sn)/Al_2O_3$ (squares). $P_{H_2}/P_{C_4H_{10}} = 9$. Ascending temperatures, closed symbols; descending temperatures, open symbols.

addition of the second metal on small supported Pt crystallites, and the obtained values were within the range observed for supported Pt.

DRIFT spectra of adsorbed CO were obtained to probe for any changes in the electronic properties of Pt after the addition of Sn or In. The main peak at 2063 cm^{-1} has been assigned to CO linearly adsorbed on small Pt particles that do not have extended crystal faces because of their small size and their morphologies, while the shoulder at 2075 cm^{-1} is due to CO linearly adsorbed on terrace sites on Pt crystal faces (62–64). This latter band was more intense for samples with larger average particle sizes (62–64). The tail around 2000 cm^{-1} was also investigated and said to be due to CO adsorption on Pt that interacts strongly with the alumina because this peak was not observed on SiO_2-supported samples (62). The band at 1835 cm^{-1} has been assigned to bridge-bonded CO (62–64).

The presence of the second metal caused some changes in the room temperature spectra. For most of the samples, there was a decrease in the frequency of the linearly bound CO at higher coverages, and this decrease was smaller for the Pt–Sn samples than for the Pt–In samples. In fact, only for the $Sn + (Pt/Al_2O_3)$ sample was there a small increase in this frequency, but this could be caused by the presence

TABLE 4

Butane Hydrogenolysis over Pt Catalysts

Catalyst	Reaction rate (mol/g/h)	TOF ($s^{-1} \times 10^2$)	Temperature sequence[a] (T_{max}, K)	E_a (kcal/mol)
Pt/Al_2O_3	4.00×10^{-3}	3.37	A (595)	35
Pt/Al_2O_3	3.37×10^{-3}	2.84	D	40
$(Pt + In)/Al_2O_3$	4.54×10^{-5}	0.0852	A (615)	28
$(Pt + In)/Al_2O_3$	1.99×10^{-5}	0.0373	D	40
$In + (Pt/Al_2O_3)$	7.42×10^{-5}	0.0964	A (615)	29
$In + (Pt/Al_2O_3)$	3.83×10^{-5}	0.0497	D	39
$Pt + (In/Al_2O_3)$	5.86×10^{-4}	0.740	A (614)	34
$Pt + (In/Al_2O_3)$	4.23×10^{-4}	0.534	D	35
$(Pt + Sn)/Al_2O_3$	1.37×10^{-3}	1.68	A (590)	43
$(Pt + Sn)/Al_2O_3$	7.05×10^{-4}	0.867	D	43
$Sn + (Pt/Al_2O_3)$	7.26×10^{-4}	0.917	A (596)	30
$Sn + (Pt/Al_2O_3)$	6.32×10^{-4}	0.798	D	29
$Pt + (Sn/Al_2O_3)$	9.02×10^{-4}	1.03	A (604)	32
$Pt + (Sn/Al_2O_3)$	6.04×10^{-4}	0.693	D	37

Note $T = 573$ K, $P_{C_4H_{10}} = 75$ Torr, $P_{H_2} = 675$ Torr.

[a] A, initial ascending temperature sequence; D, subsequent descending temperature sequence.

of slightly larger particles on that sample (65). The shift to lower wavenumbers has been observed before for several combinations of bimetallic Pt catalysts (4, 9), and it could be caused by electron transfer from the promoter atom to Pt, with an increase in the *d*-band charge transfer from Pt to the π^* antibonding orbitals of CO (9, 66). On the other hand, dilution of the platinum atoms by the second metal could also be responsible for the shift, due to an increase in the average distance between adsorbed CO molecules which would decrease dipole–dipole coupling and lower the observed vibration frequency (4, 67). Infrared spectra of CO adsorbed on Pt/Al_2O_3 and $Pt–Sn/Al_2O_3$ catalysts in which there was no change in the absorption frequency due to the presence of tin have also been published (68). These results

TABLE 5

Selectivity for *n*-butane Hydrogenolysis at 573 K on Pt Catalysts

Catalyst	Conv. (%)	C_1/C_3	S_{MET}[a]	S_{ET}[b]	S_{PROP}[c]	$S_{I\text{-}BUT}$[d]
Pt/Al_2O_3	2.8	0.97	16.5	32.0	50.9	0.6
$(Pt + In)/Al_2O_3$	0.13	1.09	14.2	39.9	39.1	5.8
$In + (Pt/Al_2O_3)$	0.16	0.87	14.7	22.1	50.6	12.6
$Pt + (In/Al_2O_3)$	0.84	0.96	14.7	35.9	46.2	3.2
$(Pt + Sn)/Al_2O_3$	2.9	0.95	14.5	37.8	45.6	2.1
$Sn + (Pt/Al_2O_3)$	1.4	0.97	15.7	32.7	48.7	2.9
$Pt + (Sn/Al_2O_3)$	2.2	0.91	15.4	32.0	50.7	1.9

Note. $P_{C_4H_{10}} = 75$ Torr, $P_{H_2} = 675$ Torr.

[a] Selectivity to methane.

[b] Selectivity to ethane.

[c] Selectivity to propane.

[d] Selectivity to isobutane.

TABLE 6

Comparison between Terminal and Central Bond Breaking

Catalyst	Temperature sequence[a]	r_t[b] (mol/h/gcat)	r_c[c] (mol/h/gcat)	E_{at}[b] (kcal/mol)	E_{ac}[c] (kcal/mol)	r_t/r_c
Pt/Al_2O_3	A	2.75×10^{-3}	1.23×10^{-3}	34	40	2.2
Pt/Al_2O_3	D	2.47×10^{-3}	8.97×10^{-4}	42	47	3.0
$(Pt + In)/Al_2O_3$	A	2.13×10^{-5}	1.64×10^{-5}	30	29	1.3
$(Pt + In)/Al_2O_3$	D	1.19×10^{-5}	7.82×10^{-6}	42	35	1.5
$Pt + (In/Al_2O_3)$	A	3.59×10^{-4}	1.97×10^{-4}	35	35	1.8
$Pt + (In/Al_2O_3)$	D	3.01×10^{-4}	9.09×10^{-5}	34	38	3.3
$In + (Pt/Al_2O_3)$	A	5.14×10^{-5}	1.45×10^{-5}	29	36	3.5
$In + (Pt/Al_2O_3)$	D	3.52×10^{-5}	1.12×10^{-5}	40	36	3.1
$(Pt + Sn)/Al_2O_3$	A	8.42×10^{-4}	4.12×10^{-4}	41	49	2.0
$(Pt + Sn)/Al_2O_3$	D	5.28×10^{-4}	1.71×10^{-4}	39	54	3.1
$Sn + (Pt/Al_2O_3)$	A	4.72×10^{-4}	2.26×10^{-4}	29	37	2.1
$Sn + (Pt/Al_2O_3)$	D	3.80×10^{-4}	1.79×10^{-4}	33	41	2.1
$Pt + (Sn/Al_2O_3)$	A	5.85×10^{-4}	2.89×10^{-4}	30	36	2.0
$Pt + (Sn/Al_2O_3)$	D	4.36×10^{-4}	1.50×10^{-4}	35	46	2.9

Note. $P_{C_4H_{10}} = 75$ Torr, $P_{H_2} = 675$ Torr.

[a] A, initial ascending temperatures; D, subsequent descending temperatures.

[b] r_t, rate of terminal bond scission at 573 K; $P_{H_2}/P_{C_4H_{10}} = 9$; E_{at}, apparent activation energy for terminal bond scission.

[c] r_c, rate of central bond scission at 573 K; $P_{H_2}/P_{C_4H_{10}} = 9$; E_{ac}, apparent activation energy for terminal bond scission.

were explained by the fact that residual chlorine ions were present that could cause a shift to higher frequencies. These results show that several simultaneous effects can influence the band position due to CO adsorbed on bimetallic catalysts. The presence of the second metal can shift the bands to lower frequencies, while the presence of residual chlorine and an increase in the particle size can shift the band to higher frequencies. Another consequence of the dilution of the surface platinum atoms in our samples is the suppression of bridged-bonded CO in some of the bimetallic samples and the suppression of the 2075 cm^{-1} shoulder. The fact that some of the Pt–Sn samples did not show this trend indicates that dilution of the surface platinum atoms is not as homogeneous in the Pt–Sn samples as it is in the Pt–In samples. The reason for the leveling out of the peak position at intermediate coverages on all the Pt–Sn catalysts is not known, but it could reflect a less homogeneous coverage of Sn on these Pt surfaces.

Figure 5 shows that at very low coverages all samples showed similar CO vibration frequencies. This demonstrates that the red shift observed for some of the bimetallic samples at saturation coverage is mainly due to dipole-dipole interactions. These results are in conformity with previous IR studies of CO on Pt–Sn catalysts, which have shown by isotopic dilution (4) or by thermal desorption methods that the CO singleton vibration does not change in the presence of Sn (67). In fact, our value of 2042 ± 3 cm^{-1} is in excellent agreement with the reported value of 2041 ± 6 cm^{-1} (67). This behavior is also very consistent with our calorimetric results, both of which indicate that the main mechanism of promotion in our samples is a geometric effect.

The turnover frequency of 0.034 s^{-1} at 573 K for *n*-butane hydrogenolysis on Pt/Al_2O_3 is somewhat higher than those reported in previous studies. The Pt/Al_2O_3 catalysts reported in the literature have given turnover frequencies (TOFs) ranging from 0.0016 to 0.027 s^{-1}, (13, 68–70), as shown in Table 8. Two values may be low because 100% dispersion for Pt was assumed in their estimation, and the lowest values may be a consequence of coke formation because the bracketing technique was not used. The activation

TABLE 7

Initial and Integral Heats of Adsorption of CO on Supported Pt

Surface	Initial Q_{ad} (kcal/mol)	Integral Q_{ad} (kcal/mol)	Ref.
Pt/Al_2O_3	18	—	56
Pt/η–Al_2O_3	—	23.9	57
Pt/η–Al_2O_3	—	21.3	8
Pt/SiO_2	—	27.0	56
Pt/SiO_2	—	29.4	8
Pt/SiO_2	38.2	34.6	58
Pt/SiO_2	28	23.4	59
Pt/SiO_2	29.9	20.3	60
Pt/SiO_2	35.8	26.6	28
$6Pt–1Sn/SiO_2$	32.3	24.3	28
$1Pt–1Sn/SiO_2$	35.8	22.3	28
$1Pt–3Sn/SiO_2$	28.7	16.7	28

TABLE 8

Butane Hydrogenolysis on Pt/Al_2O_3 Catalysts

Catalyst	TOF (10^{-2} s^{-1})	E^a (kcal/mol)	Reference
2% Pt/Al_2O_3	0.6	—	68
2% Pt/Al_2O_3	0.16	34	69
0.6% Pt/Al_2O_3	1.8[b]	33.8	13
0.3% Pt/Al_2O_3	2.2[b]	33.3	13
1.7% Pt/Al_2O_3	2.3	42	70
0.7% Pt/Al_2O_3	3.4	35	This study

[a] Values obtained at 573 K, 1 atm, $H_2/C_4H_{10} = 9$.
[b] Pt dispersion assumed to be unity.

energy of 35 kcal/mol is very consistent with reported literature values that typically were around 34 kcal/mol (Table 8).

The suppression of hydrogenolysis activity due to the addition of an inactive metal has been observed in various hydrocarbon conversions (1, 15–17). This effect has been successfully explained by the fact that hydrogenolysis reactions demand much larger ensembles of Pt atoms to occur; for example, the hydrogenolysis of *n*-butane is considered to occur via the formation of 1,2-di-σ-adsorbed butane plus adsorbed H atoms. The addition of the second metal disrupts these ensembles and decreases their size, thus suppressing hydrogenolysis reactions. Our results suggest that the nature of the promoter influences the degree of suppression, as In suppressed hydrogenolysis more effectively than Sn. Indeed, this result is in accordance with the results of Loc *et al.* (20), who observed that In was a better promoter than Sn for isobutane conversion to isobutene at 770 K as In suppressed hydrogenolysis activity. Furthermore, the DRIFTS studies of CO adsorbed on these catalysts also showed that the dilution of surface Pt atoms was more effective with In than with Sn. In the Pt–Sn samples, the bridged form of adsorbed CO was not completely suppressed, whereas in the Pt–In catalysts the band associated with the bridged form of adsorbed CO was not observed.

The sites for hydrogenolysis and isomerization consist of a critical reaction site and a secondary site. The critical site is related to the mode of hydrocarbon chemisorption (71–73), while the secondary site is related to the hydrogen chemisorption that occurs during dehydrogenation of the hydrocarbon. Two routes were identified involving the critical sites (73). The C_2 mode requires at least two adjacent surface Pt atoms and leads to central bond breaking which produces ethane. The isounit mode requires a smaller number of surface atoms (perhaps one) and favors the formation of methane and propane from butane. The selectivity toward central bond scission or terminal bond scission was not altered in these bimetallic systems. This implies that if there are different sites for each kind of bond scission, they are equally blocked in the bimetallic catalysts; i.e., there is no preferential positioning of the promoter atoms related to the platinum atoms. The effect of coking, on the other hand, was to poison preferentially the central bond scission sites, as it can be observed in Table 6 that r_t/r_c values usually went up during the sequence of descending temperatures.

SUMMARY

The effects of Sn and In on the adsorption and catalytic properties of Pt were investigated. The presence of either Sn or In decreased the adsorption capacity of platinum as measured by the hydrogen uptake at 300 K. The irreversible heats of hydrogen adsorption on the various catalysts fell between 10.6 and 13.3 kcal/mol which is within the range previously observed for platinum dispersed on various supports. The variation in the Q_{ad} values for hydrogen adsorption was not large enough to imply that the electronic properties of platinum were extensively altered, and it indicated that the main mechanism for modification of the platinum was geometric, with any electronic effects playing a minor role. The presence of the promoters also decreased the amount of CO adsorbed at 300 K, as observed for H_2; however, the irreversible heats of CO adsorption were essentially invariant with values of 23.5 ± 1.1 kcal/mol, which is consistent with values previously measured on Al_2O_3-supported Pt. Thermal desorption experiments in the DRIFTS cell showed that the singleton vibration at 300 K lay within the range of 2042 ± 3 cm^{-1} for all the samples investigated. The hydrogenolysis of butane proved to be useful in differentiating between the Sn and In additives. The specific activity for hydrogenolysis was decreased by the addition of either of the promoters, independently of the sequence of addition, but the effect of In was more pronounced and a 40-fold decrease in TOF was observed for one of the $Pt–In/Al_2O_3$ catalysts. All these results, particularly the IR and kinetic behavior, indicate that the Pt surface atoms were more homogeneously diluted or covered by In than by Sn.

ACKNOWLEDGMENTS

We thank Ashland Petroleum Company for partial support of this study. F.B.P is also grateful to CNPq (Conselho Nacional de Desenvolvimento Científico e Tecnológico) for the grant of a scholarship for a 18-month stay at the Pennsylvania State University.

REFERENCES

1. Sinfelt, J. H., "Bimetallic Catalysts: Discoveries, Concepts and Applications." Wiley, New York, 1983.
2. Gates, B., Katzer, J., and Schuit, G. C. A., "Chemistry of Catalytic Processes." McGraw–Hill, New York, 1979.
3. Ponec, V., *Adv. Catal.* **32**, 149 (1983).
4. Bastein, A. G. T. M., Toolenaar, F. J. C. M., and Ponec, V., *J. Catalysis* **90**, 88 (1984).
5. Burch, R., *J. Catal.* **71**, 348 (1981).
6. Sen, B., Chou, P., and Vannice, M. A., *J. Catal.* **101**, 517 (1986).
7. Vannice, M. A., Sen, B., and Chou, P., *Rev. Sci. Instrum.* **58**, 647 (1987).
8. Sen, B., and Vannice, M. A., *J. Catal.,* **130**, 9 (1991).

9. Palazov, A., Bonev, Ch., Kadinov, G., Shopov, D., Lietz, G., and Völter, J., *J. Catal.* **71**, 1 (1981).
10. Kempling, J. C., and Anderson, R. B., *Ind. Eng. Chem. Process Des. Dev.* **11**, 146 (1972).
11. Anderson, J. R., *Adv. Catal.* **23**, 1 (1973).
12. Leclercq, G., Leclercq, L., and Maurel, R., *J. Catal.* **44**, 68 (1976).
13. Bond, G. C., and Gelsthorpe, M. R, *J. Chem. Soc. Faraday Trans. I* **85**, 3767 (1989).
14. Abrevaya, H., and Imai, T., U. S. Patent 4608360, 1986.
15. Dautzenberg, F. M., Helle, J. N., Biloen, P., and Sachtler, W. M. H., *J. Catal.* **63**, 119 (1980).
16. Baronetti, G. T., De Miguel, S. R., Scelza, O. A., and Castro, A. A., *Appl. Catal.* **24**, 109 (1986).
17. Völter, J., *in* "Catalytic Hydrogenation" (L. Cerveny, Ed.). Elsevier, Amsterdam, 1986.
18. Davis, B. H., *in* "Proceedings of 10th International Congress on Catalysis, Budapest, 1992," Part A, p. 889. Elsevier, Amsterdam, 1993.
19. Schwank, J., Balakrishnan, K., and Sachdev, A., *in* "Proceedings of 10th International Congress on Catalysis, Budapest, 1992," Part A, p. 905. Elsevier, Amsterdam, 1993.
20. Loc, L. C., Thoang, H. S., Gaidai, N. A., and Kiperman, S. L., "Proceedings of 10th International Congress on Catalysis, Budapest, 1992," Part C, p. 2277. Elsevier, Amsterdam, 1993.
21. Bursian, N. R., Zharkov, B. B., Kogan, S. B., Lavostikin, G. A., and Podklentnova, N. M., *in* "Proceedings of 8th International Congress on Catalysis, Berlin, 1984," Vol. 2, p. 481. Dechema, Frankfurt-am-Main, 1984.
22. Venter, J. J., and Vannice, M. A., *Appl. Spectrosc.* **42**, 1096 (1988).
23. Vannice, M. A., Twu, C. C., and Moon, S. H., *J. Catal.* **79**, 70 (1983).
24. Primet, M., *J. Catal.* **88**, 273 (1984).
25. Meitzner, G., Via, G. H., Lytle, F. W., Fung, S. C., and Sinfelt, J. H., *J. Phys. Chem.* **92**, 2925 (1988).
26. Hobson, M. C., Jr., Goresh, S. L., and Khare, G. P., *J. Catal.* **142**, 641 (1993).
27. Passos, F. B., Silva, P. R. J., Saitovitch, H., and Schmal, M., *Hyperfine Interact.* **84**, 563 (1994).
28. Cortright, R. D., and Dumesic, J. D., *J. Catal.* **148**, 771 (1994).
29. Lantz, J. B., and Gonzalez, R. D., *J. Catal.* **41**, 293 (1976).
30. Goddard, S. A., Amiridis, M. D., Rekoske, J. E., Cardona-Martinez, N., and Dumesic, J. A., *J. Catal.* **117**, 155 (1989).
31. Lu, K. E., and Rye, R. R., *Surf. Sci.* **45**, 677 (1974).
32. Norton, P. R., Davies, J. A., and Jackman, T. E., *Surf. Sci.* **121**, 103 (1982).
33. Christman, K., Ertl, G., and Pignet, T., *Surf. Sci.* **54**, 365 (1976).
34. Mc Cabe, R. W., and Schmidt, L. D., *in* "Proceedings, 7th International Vacuum Congress, Vienna, 1977," p. 1201.
35. Nieuwenhuys, B. E., *Surf. Sci.* **59**, 430 (1976).
36. Weinberg, W. H., Monroe, D. R., Lampton, V., and Merrill, R. P., *J. Vac. Sci. Technol.* **14**, 444 (1977).
37. Netzer, F. P., and Kneringer, G., *Surf. Sci.* **51**, 526 (1975).
38. Stephan, J. J., Ponec, V., and Sachtler, W. M. H., *J. Catal.* **37**, 81 (1975).
39. Cerny, S., Smutek, M., and Buztek, F., *J. Catal.* **38**, 245 (1975).
40. Paffett, M. T., Gebhard, S. C., Windham, R. G., and Koel, B. E., *J. Phys. Chem.* **94**, 6831 (1990).
41. Norton, P. R., Goodale, J. W., and Selkirk, E. B., *Surf. Sci.* **66**, 101 (1977).
42. Mc Cabe, R. W., and Schmidt, L. D., *Surf. Sci.* **66**, 101 (1977).
43. Ertl, G., Neumann, M., and Streit, K. M., *Surf. Sci.* **64**, 393 (1977).
44. Steininger, H., Ibach, H., and Lehwald, S., *Surf. Sci.* **123**, 264 (1982).
45. Poelsema, B., Palmer, R. L., and Comsa, G., *Surf. Sci.* **123**, 152 (1982).
46. Thiel, P. A., Behm, R. J., Norton, P. R., and Ertl, G., *Surf. Sci.* **121**, L533 (1982).
47. Barteau, M. A., Ko, E. I., and Madix, R. J., *Surf. Sci.* **102**, 99 (1981).
48. Jackman, T. E., Davies, J. A., Jackson, D. P., Unertl, W. N., and Norton, P. R., *Surf. Sci.* **120**, 389 (1982).
49. Fair, J., and Madix, R. J., *J. Chem. Phys.* **73**, 3480 (1980).
50. Bonzel, H. P., and Ku, R. J., *J. Chem. Phys.* **58**, 4617 (1973).
51. Comrie, C. M., and Lambert, R. M., *J. Chem. Soc. Faraday Trans 1* **72**, 1659 (1976).
52. Park, Y. O., Banholzer, W. F., and Masel, R. I., *Surf. Sci.* **155**, 341 (1985).
53. Mc Clellan, M. R., Gland, J. L., and Mc Feely, F. R., *Surf. Sci.* **112**, 63 (1981).
54. Collins, D. M., and Spicer, W. E., *Surf. Sci.* **69**, 85 (1977).
55. Brennan, D., and Hayes, F. H., *Philos. Trans. R. Soc. A.* **258**, 347 (1965).
56. Vannice, M. A., Hasselbring, L. C., and Sen, B., *J. Catal.* **97**, 66 (1986).
57. Herz, R. K., and Mc Cready, D. F., *J. Catal.* **81**, 358 (1983).
58. Auckett, P. N., *in* "Structure and Reactivity of Surfaces" (C. Morterra *et al.*, Eds.), p. 11. Elsevier, Amsterdam, 1989.
59. Goddard, S. A., Amiridis, M. D., Rekoske, J. E., Cardona-Martinez, N., and Dumesic, J. A., *J. Catal.* **117**, 155 (1989).
60. Efremov, A. A., Bakhnmutova, N. I., Pankratiev, Yu. D., and Kuznetsov, B. N., *React. Kinet. Catal. Lett.* **28**, 103 (1985).
61. Verbeek, H., and Sachtler, W. M. H., *J. Catal.* **42**, 257 (1976).
62. Barth, R., Pitchai, R., Anderson, R. L., and Verykios, X. E., *J. Catal.* **116**, 61 (1989).
63. Haaland, D. M., *Surf. Sci.* **185**, 1 (1985).
64. Barth, R., and Ramachandran, A., *J. Catal.* **125**, 467 (1990).
65. Solomennikov, A. A., Lokhov, Yu. A., Davydov, A. A., and Ryndin, Yu. A., *Kinet. Katal.* **20**, 714 (1979).
66. Blyholder, G., *J. Phys. Chem.* **68**, 2772 (1964).
67. Balakrishnan, K., and Schwank, J., *J. Catal.* **138**, 491 (1992).
68. Leclercq, G., Leclercq, L., and Maurel, R., *J. Catal.* **50**, 87 (1977).
69. Betizeau, C., Leclercq, G., Maurel, R., Bolivar, C., Charcosset, H., Fréty, R., and Tournayan, L., *J. Catal.* **45**, 179 (1976).
70. Nazimeck, D., and Ryczkowski, J., *React. Kinet. Catal. Lett.* **40**, 145 (1989).
71. Martin, G. A., *J. Catal.* **60**, 345 (1979).
72. Frennet, A., Lienard, G., Crucqu, F., and Degols, F., *J. Catal.* **53**, 150 (1978).
73. Foger, K., and Anderson, J. R., *J. Catal.* **64**, 448 (1980).